Original paper

Automatic reconstruction of interstitial needles using CT images in post-operative cervical cancer brachytherapy based on deep learning

Hongling Xie, MD[1]*, Jiahao Wang, MD[1]*, Yuanyuan Chen, MD[1], Yeqiang Tu, MD[1], Yukai Chen, MD[1], Yadong Zhao[1], Pengfei Zhou[1], Shichun Wang[2], Zhixin Bai[2], Qiu Tang, PhD[1]

[1]Department of Radiation Oncology, Women's Hospital, School of Medicine, Zhejiang University, Hangzhou, Zhejiang, China, [2]Hangzhou Ruicare MedTech Co., Ltd., Hangzhou, Zhejiang, China

*Hongling Xie and Jiahao Wang contributed equally to this work.

Abstract

Purpose: The purpose of this study was to investigate the precision of deep learning (DL)-based auto-reconstruction in localizing interstitial needles in post-operative cervical cancer brachytherapy (BT) using three-dimensional (3D) computed tomography (CT) images.

Material and methods: A convolutional neural network (CNN) was developed and presented for automatic reconstruction of interstitial needles. Data of 70 post-operative cervical cancer patients who received CT-based BT were used to train and test this DL model. All patients were treated with three metallic needles. Dice similarity coefficient (DSC), 95% Hausdorff distance (95% HD), and Jaccard coefficient (JC) were applied to evaluate the geometric accuracy of auto-reconstruction for each needle. Dose-volume indexes (DVI) between manual and automatic methods were used to analyze the dosimetric difference. Correlation between geometric metrics and dosimetric difference was evaluated using Spearman correlation analysis.

Results: The mean DSC values of DL-based model were 0.88, 0.89, and 0.90 for three metallic needles. Wilcoxon signed-rank test indicated no significant dosimetric differences in all BT planning structures between manual and automatic reconstruction methods ($p > 0.05$). Spearman correlation analysis demonstrated weak link between geometric metrics and dosimetry differences.

Conclusions: DL-based reconstruction method can be used to precisely localize the interstitial needles in 3D-CT images. The proposed automatic approach could improve the consistency of treatment planning for post-operative cervical cancer brachytherapy.

J Contemp Brachytherapy 2023; 15, 2: 134-140
DOI: https://doi.org/10.5114/jcb.2023.126514

Key words: deep learning, interstitial needles, brachytherapy, cervical cancer.

Purpose

Cervical cancer is the fourth most frequently diagnosed cancer, and the fourth leading cause of cancer-related deaths in women around the world [1]. External beam radiation therapy (EBRT) and brachytherapy (BT) are effective treatments for cervical cancer [2, 3]. The American Brachytherapy Society (ABS) recommends post-operative adjuvant BT for non-radical surgery, close or positive margins, large or deeply invasive tumors, and parametrial or vaginal involvement [4]. Several reports supported that vaginal cuff BT boost was associated with a reduced recurrence rate in post-operative setting of high-risk patients with early-stage cervical cancer [5, 6]. Currently, the application of 3D image-guided BT (IGBT) allows adaptive treatment planning process, and presents more advantageous, compared with conventional two-dimensional (2D), image-based method [7]. Meanwhile, applicator reconstruction is critical step during the procedure of IGBT treatment planning [8].

The accuracy of applicators reconstruction has significant impact on dosimetric results of IGBT treatment plan because of steep dose gradients [9-11]. In general, applicators reconstruction are mostly performed manually by physicists. The localization process is a time-consuming part in IGBT workflow [12], and always suffers from subjective variability. Therefore, it is strongly needed to achieve automatic applicator reconstruction in IGBT workflow to ensure treatment planning accuracy, consistency, and efficiency.

In recent years, deep learning (DL)-based frameworks have been applied in radiotherapy (RT) and achieved

Address for correspondence: Dr. Qiu Tang, Department of Radiation Oncology, Women's Hospital, School of Medicine, Zhejiang University, Hangzhou 310006, Zhejiang, China, phone: +86-13705811850, ✉ e-mail: qiutang@zju.edu.cn

Received: 02.11.2022
Accepted: 27.03.2023
Published: 06.04.2023

superior results, including automatic segmentation of target volume and organs at risk [13], automatic RT planning [14], and prediction of irradiation toxicity and prognosis [15]. The advantage of DL is the ability to recognize novel scenes by automatically extracting labeled features through learning of generalized features in training samples [16-18]. Deep learning plays a major role in brachytherapy [19]; some studies have focused on the automatic applicators reconstruction in IGBT workflow based on DL methods [20-27]. However, geometric metrics and subjective assessment were always selected to evaluate the performance of DL models in previous studies, with few studies reporting dosimetric differences in auto-reconstruction of applicators.

The purpose of the present study was to evaluate the accuracy of DL model in automatic reconstruction of metallic interstitial needles in patients with post-operative cervical cancer using both geometric and dosimetric metrics in IGBT workflow.

Material and methods

The work flowchart of this study is illustrated in Figure 1, and three key steps summarized the procedure. Firstly, the experienced physicist annotated metallic needles as the standard applicators reconstruction. Secondly, the DL-based model was trained and verified by the standard data, and automatic reconstructions of interstitial needles was generated. Thirdly, the accuracy of DL-based auto-reconstruction was assessed using geometric metrics and dosimetric differences.

Data annotation

Data of seventy post-operative cervical cancer patients collected between August, 2021 and July, 2022 were used in this study. In all patients, three interstitial needles were employed, with a prescription dose of 12-30 Gy (6 Gy/fraction). CT images of 70 patients were reconstructed with 512 × 512 matrix size and 3 mm slice thickness using a Philips Brilliance Big Bore CT scanner system (Philips Healthcare, Best, The Netherlands). The number of CT slices ranged from 69 to 118. Interstitial needles were delineated manually by an intern physicist using Oncentra treatment planning system, version 4.3 (Elekta AB, Stockholm, Sweden), and named 1, 2, and 3. To establish standard delineation, all the manual needles were evaluated and approved by a senior physicists.

Deep learning-based auto-reconstruction

We presented an adaptive DL model based on nnU-Net (no-new-Net) to reconstructed needles for post-operative cervical cancer BT. Figure 2 depicts the design concept for DL model used in the study. The nnU-Net [28] defines dataset fingerprint and pipeline fingerprint. Pipeline fingerprints are classified into three categories, including blueprint, inferred, and empirical parameters. A 2D U-Net, 3D U-Net, and 3D U-Net cascade are the three U-Net configurations that nnU-Net generates by default. 2D U-Net and 3D U-Net are input full resolution images, while 3D U-Net cascade firstly uses a low resolution image for coarse segmentation, and then applies a full resolution image for fine segmentation.

In this work, we mainly focused on the 3D U-Net for reconstruction of the applicator due to 3D-CT images with high resolution of metallic needles in our datasets. The 70 patients were separated into training, validating, and testing data in the ratio of 50 : 10 : 10. To improve image contrast and improve the interstitial needles display, histogram equalization processing on CT scans from training and validating data was performed using digital image processing software.

Geometric assessment

Geometric correctness of the interstitial needles was compared using DSC, 95% HD, and JC [29]. DSC and JC calculated spatial overlap between two regions as follows:

$$DSC = 2\,|A \cap B|\,/\,(|A| + |B|),$$

$$JC = |A \cap B|\,/\,|A \cup B|,$$

where A and B are manually segmented regions or auto-segmented regions based on DL. For the complete overlap, the values of DSC and JC are 1. For the incomplete overlap, the values of DSC and JC are close to 0.

Hausdorff distance (HD) was used to quantify the accuracy of digitized needle trajectories. In order to exclude outlier distance values, 95% HD was chosen to indicate the largest surface-to-surface separation among the closest 95% of surface points. Unit of HD95 was mm.

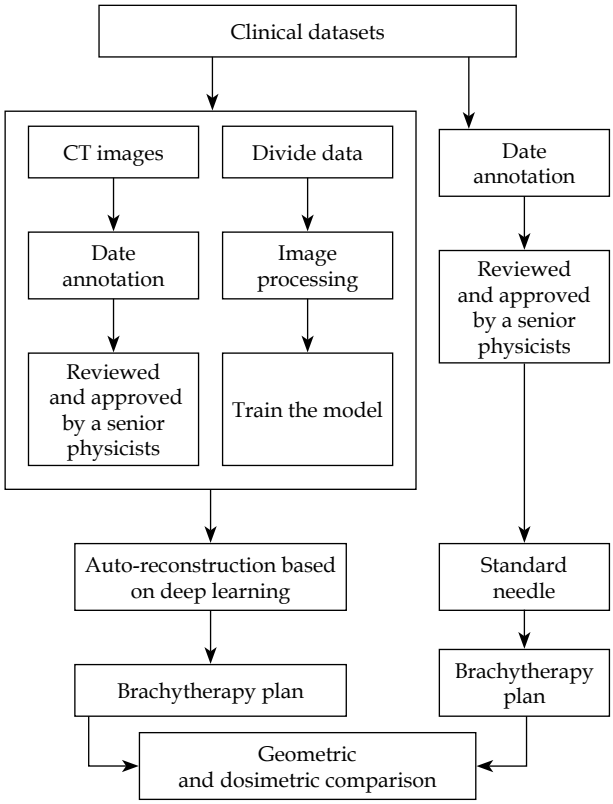

Fig. 1. Flowchart of manual and deep learning (DL)-based auto-reconstruction evaluation experiment. Brachytherapy plans were designed and optimized based on standard and auto-reconstructed needles for dosimetric evaluation

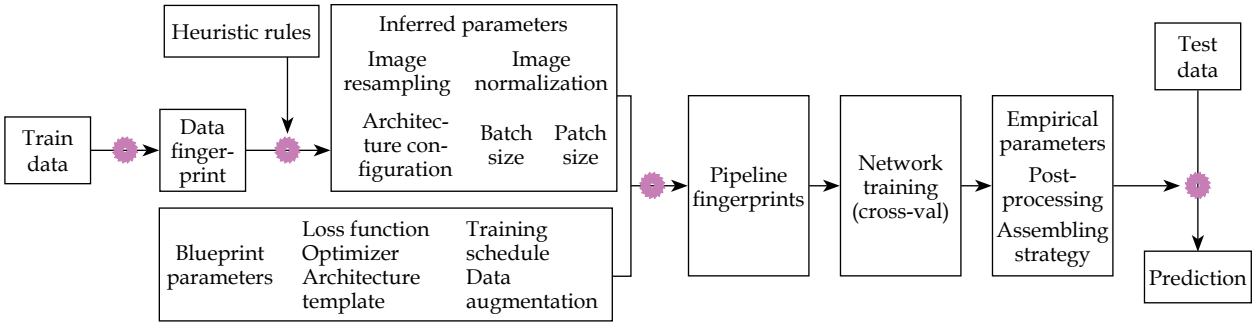

Fig. 2. Design of the nnU-Net

The smaller the HD95, the better the segmentation. Hausdorff distance (HD) was computed as:

$$HD = \max (h(A, B), h(B, A)),$$

With h defined as $h(A, B) = \max_{a \in A} \min_{b \in B} d(a, b)$, where a and b are the points on the surfaces of A and B.

Dosimetric comparison

Oncentra treatment planning system was applied to compute and optimize BT plans (original plan), based on standard manual needles. Radio-active source position and time were migrated from the original plans to the automatic reconstruction needles to generate DL plans. Dose volume histogram (DVH) was used to investigate the dosimetric difference between original plans and DL plans. For high-risk clinical target volume (HR-CTV), we mainly focused on $D_{90\%}$, $D_{98\%}$ (D_{98} and D_{90} were doses to 98% and 90% of HR-CTV volume, respectively). For organs at risk (OARs), we mainly focused on D_{2cc}, D_{1cc}, and $D_{0.1cc}$. Dose values of D_{2cc}, D_{1cc}, and $D_{0.1cc}$ represented 2 cc, 1 cc and 0.1 cc volumes of OARs that received the maximum dose, respectively. OARs included the bladder, rectum, sigmoid colon, and small intestine.

Statistical analysis

IBM SPSS statistics software (version 26.0, IBM Inc., Armonk, NY, USA) was used for statistical analysis, where

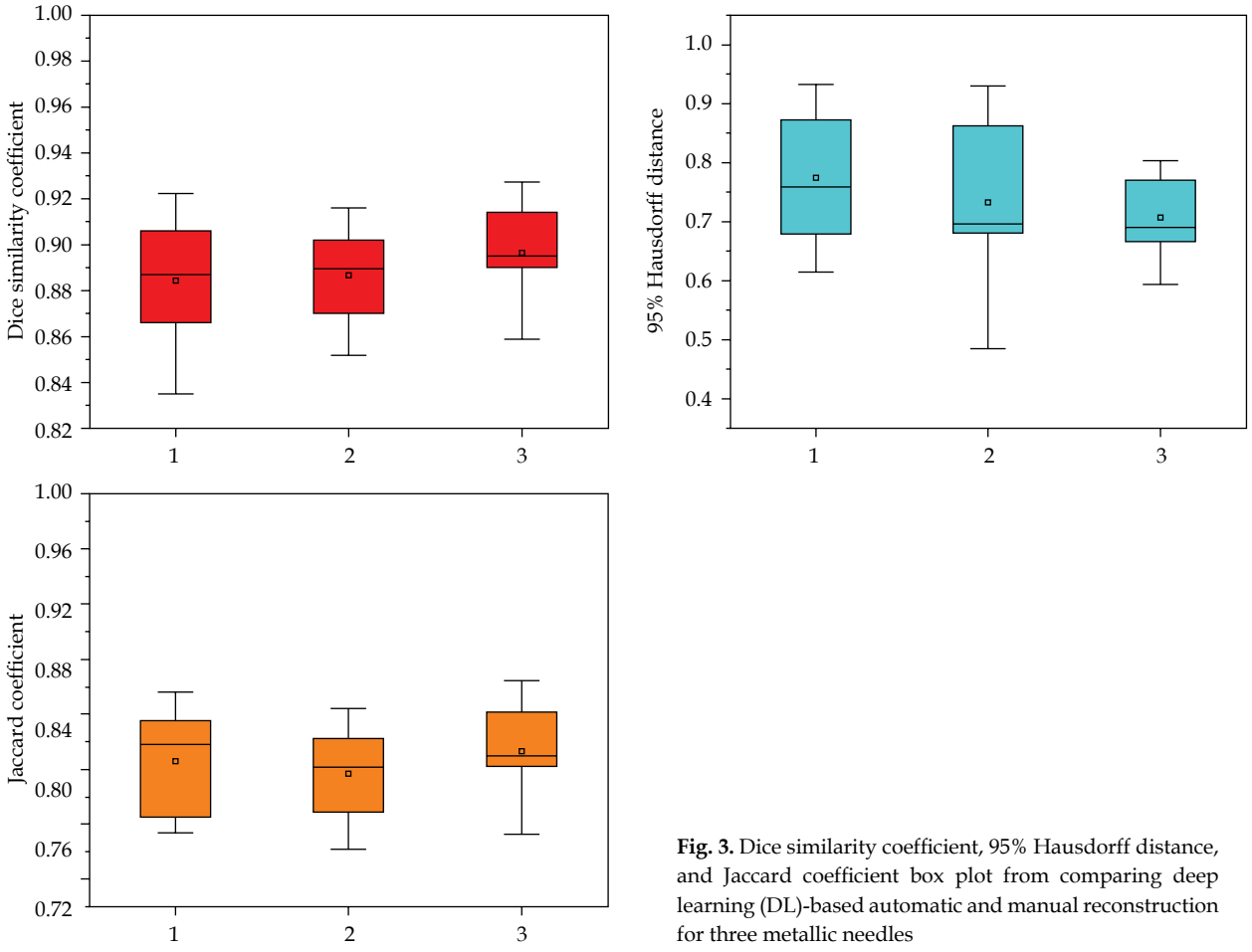

Fig. 3. Dice similarity coefficient, 95% Hausdorff distance, and Jaccard coefficient box plot from comparing deep learning (DL)-based automatic and manual reconstruction for three metallic needles

mean ± standard deviation (SD) was applied for presenting and summarizing the results. Wilcoxon's paired non-parametric signed-rank test was used to compare the dosimetric difference between two methods, $p < 0.05$ indicated that the difference was statistically significant. Spearman's correlation analysis was applied to assess the relationships between geometric metrics and dosimetric difference.

Results

Evaluation of geometric metrics

The geometric accuracy of DL auto-reconstruction of metallic needles is presented in Figure 3. Automatic reconstruction produced the results for three needles, with average DSC value of 0.88 ±0.03, 0.89 ±0.02, and 0.9 ±0.02, respectively; 95% HD of 0.77 ±0.12 mm, 0.73 ±0.13 mm, and 0.71 ±0.07 mm, respectively; and JC of 0.81 ±0.04, 0.8 ±0.34, and 0.81 ±0.03, respectively.

Evaluation of dosimetric metrics

Table 1 demonstrates the comparisons of dosimetric parameters between two methods using Wilcoxon's paired non-parametric signed-rank test. There were no statistically significant dosimetric differences for all of the BT planning structures ($p > 0.05$). Figure 4 illustrates 3D views of three metallic needles for manual and automatic reconstructions. The reconstructions of applicators with DL model were in good agreement with the manual approach. Examples of dose distributions from manual and DL-based methods are shown in Figure 5.

Correlation analysis between geometric and dosimetric metrics

The results of Spearman correlation analysis between geometric metrics and dosimetric metrics (Δdose) are presented in Table 2. The correlation analysis demonstrated weak link between all of the dosimetric

Table 1. Dosimetric comparisons between two methods in brachytherapy treatment plans

Structure	Geometric parameters	Manual delineation	Automatic delineation	Differences (%)	*Z*	*P*-value
		Mean ± standard deviation				
HR-CTV	D_{90} (cGy)	663.45 ±12.98	661.03 ±12.68	0.36	–0.255	0.799
	D_{98} (cGy)	663.45 ±12.98	562.69 ±17.93	0.63	–0.561	0.575
Bladder	D_{2cc} (cGy)	269.13 ±53.36	269.92 ±53.13	–0.29	–0.561	0.575
	D_{1cc} (cGy)	299.32 ±59.24	300.22 ±59.22	–0.30	–0.561	0.575
	$D_{0.1cc}$ (cGy)	367.56 ±74.66	368.35 ±75.23	–0.21	–0.408	0.683
Rectum	D_{2cc} (cGy)	304.05 ±27.19	299.83 ±29.11	1.39	–1.682	0.093
	D_{1cc} (cGy)	350.75 ±33.94	339.88 ±35.76	3.10	–1.784	0.074
	$D_{0.1cc}$ (cGy)	460.81 ±72.48	437.44 ±66.07	5.07	–1.784	0.074
Sigmoid	D_{2cc} (cGy)	85.94 ±38.31	85.60 ±37.98	0.40	–0.764	0.445
	D_{1cc} (cGy)	100.69 ±53.76	100.29 ±53.04	0.40	–0.663	0.508
	$D_{0.1cc}$ (cGy)	142.50 ±93.38	141.44 ±91.04	0.74	–0.968	0.333
Intestine	D_{2cc} (cGy)	81.11 ±54.82	81.48 ±56.08	–0.46	–0.255	0.799
	D_{1cc} (cGy)	92.61 ±65.80	93.42 ±68.24	–0.87	–0.051	0.959
	$D_{0.1cc}$ (cGy)	124.29 ±94.70	125.69 ±98.85	–1.13	–0.338	0.735

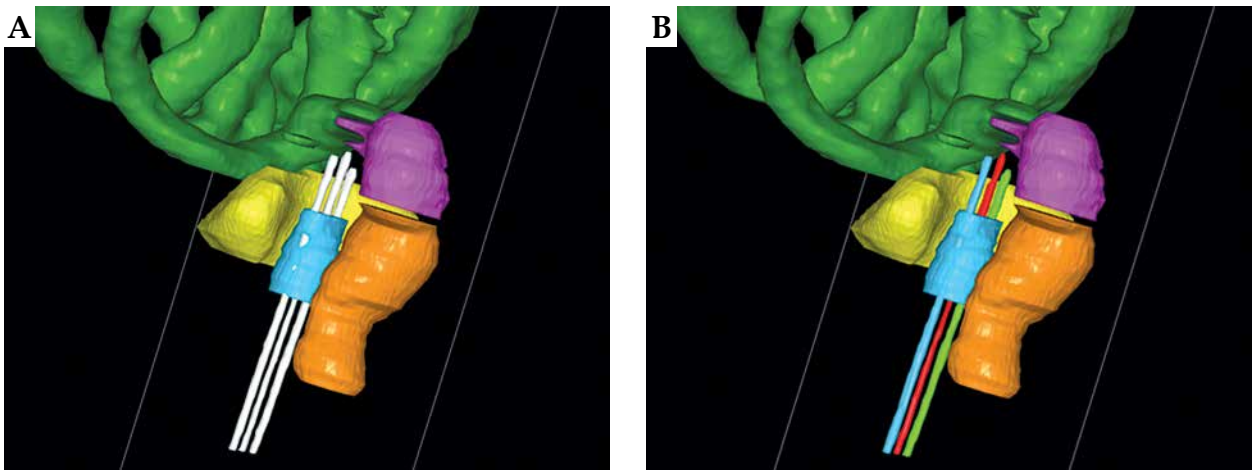

Fig. 4. 3D views of three metallic needles for manual and automatic reconstructions. The three white needles were manually reconstructed by a physicists. The red, blue and green needles were automatically reconstructed based on the deep learning (DL) model

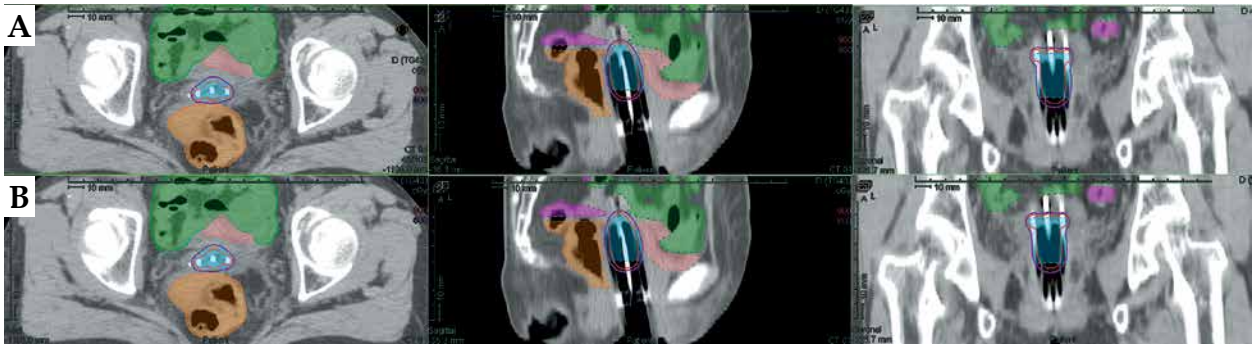

Fig. 5. Examples of dose distributions from manual and deep learning (DL)-based methods. **A**) Dosimetric results with manual reconstruction of the needles. **B**) Dosimetric results with automatic reconstruction of the needles. Purple lines represent dose distributions with 100% (600 cGy) prescription. Red lines represent dose distributions with 150% (900 cGy) prescription. Blue in the picture represents HR-CTV

difference and its geometric metrics in the BT planning structures.

Discussion

Brachytherapy is the key aspect of treatment for post-operative cervical cancer with high-risk factors. 3D-IGBT technology can produce the optimal dose distribution in target regions, and decrease the radiation dose to healthy tissues [30]. However, IGBT procedures with increasing real-time steps require more technical and manpower resources. The applicator reconstruction is one of the real-time steps in the design of 3D-IGBT plan, and the reconstruction accuracy is always dependent on the experience and subjective assessment of physicists. This highlights the importance of a rapid and accurate reconstruction method, which would improve the IGBT workflow through automation. In this work, we proposed a DL-based model for automatic needle reconstruction during CT image interstitial IGBT treatment planning.

Various applicators are used for implantation before IGBT planning, such as intra-uterine and ovoid tubes, vaginal applicator, ring applicator, interstitial needle, etc. Using different methods or DL models would generate different reconstruction results for a specific applicator. We summarized auto-segmentation results for applicators in brachytherapy from other published literature. The comparison of DSC and HD for different methods is presented in Table 3. Image thresholding and density-based clustering were applied to segment the tandem and ovoids applicator, and HD was ≤ 1 mm [31]. A DSD-U-Net model [26] was proposed to reconstruct the intra-uterine and ovoid tubes, and achieved average DSC value of 0.92. A U-Net model [32] was used to automatically segment Fletcher applicator with average DSC value of 0.89. A 2D U-Net algorithm [33] was tested to reconstruct the needles, with average DSC value of 0.59 and HD value of 4.2 mm, based on MR images. Two phases DL-based segmentation and object-tracking algorithms were adopted to reconstruct the interstitial needles in CT-guided prostate brachytherapy. In a study [34], DSC between the network output and the ground truth was 0.95. In the present work, the nnU-Net model was trained and reconstructed the metallic needles with average DSC value of 0.89, and

Table 2. Correlations between geometric metrics and dosimetric differences

Structure	Geometric parameters	DSC		95% HD		JC	
		R	*p*-value	*R*	*p*-value	*R*	*p*-value
HR-CTV	D_{90}	–0.176	0.627	0.404	0.247	–0.239	0.507
	D_{98}	–0.185	0.609	0.429	0.216	–0.092	0.800
Bladder	D_{2cc}	–0.122	0.738	0.264	0.460	–0.238	0.509
	D_{1cc}	–0.117	0.748	0.261	0.467	–0.230	0.523
	$D_{0.1cc}$	–0.300	0.399	0.408	0.242	–0.490	0.240
Rectum	D_{2cc}	–0.302	0.397	0.361	0.305	–0.029	0.937
	D_{1cc}	–0.011	0.976	0.200	0.580	0.080	0.827
	$D_{0.1cc}$	0.385	0.272	0.154	0.671	0.124	0.732
Sigmoid	D_{2cc}	0.041	0.910	–0.110	0.763	–0.082	0.822
	D_{1cc}	–0.060	0.870	–0.070	0.848	–0.187	0.606
	$D_{0.1cc}$	–0.146	0.688	–0.096	0.792	–0.240	0.504
Intestine	D_{2cc}	–0.234	0.515	0.131	0.719	–0.373	0.289
	D_{1cc}	–0.226	0.530	0.009	0.979	–0.311	0.382
	$D_{0.1cc}$	–0.260	0.496	0.048	0.894	–0.341	0.335

Table 3. Summary of auto-segmentation results for applicators in brachytherapy from other published literature

Author(s) [Ref.]	Methods or DL models	Image type	Applicators	Enrolled patients	Results
Deufel *et al*. [31]	Image thresholding and density-based	CT	Tandem and ovoid	10 patients from Mayo Clinic for testing	DSC not used; HD ≤ 1 mm
Zhang *et al*. [26]	DSD-U-Net	CT	Tandem and ovoid	91 cases from Tianjin Medical University Cancer Institute and Hospital; 32 internal cases for testing	DSC: 0.92; HD: 2.3 mm
Hu *et al*. [32]	U-Net	CT	Fletcher	60 cases from Sichuan Cancer Hospital; 10 independent cases for testing	DSC: 0.89; HD: 1.66 mm
Shaaer *et al*. [33]	2D U-Net	MRI	Interstitial plastic needles	20 cases from Odette Cancer Centre; Odette Cancer Centre	DSC: 0.59; HD: 0.42 mm
Mohammad Mahdi *et al*. [34]	Two-phase DL models	CT	Interstitial plastic needles	25 cases from Shohada-eTajrish Educational Hospital; 5 internal cases for testing	DSC: 0.95; HD not used
Our method	nnU-Net (3D)	CT	Interstitial metal needles	70 cases from Women's Hospital in China; 10 internal cases for testing	DSC: 0.89; HD: 0.74 mm

95% HD value of 0.74 mm based on CT images. Compared with the type of tandem and ovoid applicator, the type of needle applicator is more difficult for location due to its slender shape (about 2 cc) in 3D images. Peroni [35] reported a range of DSC values that generally denoted good agreement depending on structure volume, such as the agreement of DSC value of 0.4-0.6, when the structure volume is 1-5 cc. Evidently, our DL model obtained superior geometric accuracy of needles reconstruction. This mainly benefits form the cross-validation of nnU-Net, and achieves the best ensemble during training process.

Dosimetric evaluation is necessary for automatic reconstruction in IGBT workflow. Yoganathan *et al*. [36] demonstrated the importance of dosimetric evaluation over geometric evaluation for an automatic problem in cervical cancer BT. Schindel *et al*. [37] reported that the reconstruction uncertainty could cause dosimetry change greater than 10% for MRI-based BT. Therefore, we compared the dose distribution between standard original BT plan and DL plan for every planning structure. Wilcoxon signed-rank test indicated no significant dosimetric differences in HR-CTV and OARs between the two methods. Meanwhile, Spearman correlation analysis showed weak link between geometric metrics and dosimetric differences. This might prove the automatic reconstructions of metallic needles are an alternative to the manual operation.

In this work, we investigated the performance of DL-based automatic reconstruction of metal needles in post-operative cervical cancer patients treated with IGBT. Furthermore, automatic method would improve the accuracy and efficiency, and decrease the uncertainties in adaptive IGBT process. Moreover, the application of intelligent methods may promote the development of BT, and auto-reconstruction of applicator is one of the essential tasks in the component of fully automatic IGBT plan.

There are still several limitations in this study. First, this auto-reconstruction approach may not be suitable for other situations, such as vaginal applicator or Fletcher applicator. The reason was mainly caused by single-training dataset in our DL-based model, and increasing the amount of training data including various applicators in IGBT workflow could make the DL model more robust. Second, the model was developed and evaluated based on CT images. The ability of DL-based model lacks evaluation of other imaging modalities. For different imaging settings, re-training of the DL model is recommended to ensure similar performance.

Conclusions

This study has demonstrated that our DL-based reconstruction method can be used to precisely localize metal interstitial needles in post-operative cervical cancer IGBT with 3D-CT images. The proposed automatic approach can reduce the variability and relieve physicists from the labor-intensive tasks.

Disclosure

The authors report no conflict of interest.

References

1. Sung H, Ferlay J, Siegel RL et al. Global Cancer Statistics 2020: GLOBOCAN estimates of incidence and mortality worldwide for 36 cancers in 185 countries. *CA Cancer J Clin* 2021; 71: 209-249.
2. Prescribing, recording, and reporting brachytherapy for cancer of the cervix. *J ICRU* 2013; 13: NP.
3. Tanderup K, Eifel PJ, Yashar CM et al. Curative radiation therapy for locally advanced cervical cancer: brachytherapy is NOT optional. *Int J Radiat Oncol Biol Phys* 2014; 88: 537-539.

4. Lai YL, Jin YN, Wang X et al. The case selection for vaginal cuff brachytherapy in cervical cancer patients after radical hysterectomy and external beam radiation therapy. *Front Oncol* 2021; 11: 685972.
5. Li L, Kou X, Feng X et al. Postoperative external beam irradiation with and without brachytherapy in pelvic node-positive IB1-IIA2 cervical cancer patients: a retrospective clinical study. *Radiat Oncol* 2015; 10: 189.
6. Mauro GP, Kleine RT, da Costa SCS et al. Vaginal cuff brachytherapy in the adjuvant setting for patients with high-risk early-stage cervical cancer. *Brachytherapy* 2019; 18: 747-752.
7. Suzumura EA, Gama LM, Jahn B et al. Effects of 3D image-guided brachytherapy compared to 2D conventional brachytherapy on clinical outcomes in patients with cervical cancer: A systematic review and meta-analyses. *Brachytherapy* 2021; 20: 710-737.
8. Hellebust TP, Kirisits C, Berger D et al. Recommendations from Gynaecological (GYN) GEC-ESTRO Working Group: considerations and pitfalls in commissioning and applicator reconstruction in 3D image-based treatment planning of cervix cancer brachytherapy. *Radiother Oncol* 2010; 96: 153-160.
9. Tanderup K, Hellebust TP, Lang S et al. Consequences of random and systematic reconstruction uncertainties in 3D image based brachytherapy in cervical cancer. *Radiother Oncol* 2008; 89: 156-163.
10. Kim Y, Muruganandham M, Modrick JM et al. Evaluation of artifacts and distortions of titanium applicators on 3.0-Tesla MRI: feasibility of titanium applicators in MRI-guided brachytherapy for gynecological cancer. *Int J Radiat Oncol Biol Phys* 2011; 80: 947-955.
11. Wu A, Tang D, Wu A et al. Comparison of the dosimetric influence of applicator displacement on 2D and 3D brachytherapy for cervical cancer treatment. *Technol Cancer Res Treat* 2021; 20: 15330338211041201.
12. Mayadev J, Qi L, Lentz S et al. Implant time and process efficiency for CT-guided high-dose-rate brachytherapy for cervical cancer. *Brachytherapy* 2014; 13: 233-239.
13. Jiang X, Wang F, Chen Y et al. RefineNet-based automatic delineation of the clinical target volume and organs at risk for three-dimensional brachytherapy for cervical cancer. *Ann Transl Med* 2021; 9: 1721.
14. Shen C, Chen L, Gonzalez Y, Jia X. Improving efficiency of training a virtual treatment planner network via knowledge-guided deep reinforcement learning for intelligent automatic treatment planning of radiotherapy. *Med Phys* 2021; 48: 1909-1920.
15. Deist TM, Dankers F, Valdes G et al. Machine learning algorithms for outcome prediction in (chemo)radiotherapy: An empirical comparison of classifiers. *Med Phys* 2018; 45: 3449-3459.
16. Larentzakis A, Lygeros N. Artificial intelligence (AI) in medicine as a strategic valuable tool. *Pan Afr Med J* 2021; 38: 184.
17. Connor CW. Artificial intelligence and machine learning in anesthesiology. *Anesthesiology* 2019; 131: 1346-1359.
18. Gupta R, Srivastava D, Sahu M et al. Artificial intelligence to deep learning: machine intelligence approach for drug discovery. *Mol Divers* 2021; 25: 1315-1360.
19. Fechter T, Sachpazidis I, Baltas D. The use of deep learning in interventional radiotherapy (brachytherapy): A review with a focus on open source and open data. *Z Med Phys* 2022; S0939-3889(22)00099-X.
20. Jung H, Gonzalez Y, Shen C et al. Deep-learning-assisted automatic digitization of applicators in 3D CT image-based high-dose-rate brachytherapy of gynecological cancer. *Brachytherapy* 2019; 18: 841-851.
21. Jung H, Shen C, Gonzalez Y et al. Deep-learning assisted automatic digitization of interstitial needles in 3D CT image based high dose-rate brachytherapy of gynecological cancer. *Phys Med Biol* 2019; 64: 215003.
22. Shen C, Gonzalez Y, Klages P et al. Intelligent inverse treatment planning via deep reinforcement learning, a proof-of-principle study in high dose-rate brachytherapy for cervical cancer. *Phys Med Biol* 2019; 64: 115013.
23. Dai X, Lei Y, Zhang Y et al. Automatic multi-catheter detection using deeply supervised convolutional neural network in MRI-guided HDR prostate brachytherapy. *Med Phys* 2020; 47: 4115-4124.
24. Gillies DJ, Rodgers JR, Gyacskov I et al. Deep learning segmentation of general interventional tools in two-dimensional ultrasound images. *Med Phys* 2020; 47: 4956-4970.
25. Golshan M, Karimi D, Mahdavi S et al. Automatic detection of brachytherapy seeds in 3D ultrasound images using a convolutional neural network. *Phys Med Biol* 2020; 65: 035016.
26. Zhang D, Yang Z, Jiang S et al. Automatic segmentation and applicator reconstruction for CT-based brachytherapy of cervical cancer using 3D convolutional neural networks. *J Appl Clin Med Phys* 2020; 21: 158-169.
27. Weishaupt LL, Sayed HK, Mao X et al. Approaching automated applicator digitization from a new angle: Using sagittal images to improve deep learning accuracy and robustness in high-dose-rate prostate brachytherapy. *Brachytherapy* 2022; 21: 520-531.
28. Isensee F, Petersen J, Klein A et al. nnU-Net: self-adapting framework for U-Netbased medical image segmentation. arXiv:180910486, 2018.
29. Yeghiazaryan V, Voiculescu I. Family of boundary overlap metrics for the evaluation of medical image segmentation. *J Med Imaging (Bellingham)* 2018; 5: 015006.
30. Potter R, Haie-Meder C, Van Limbergen E et al. Recommendations from gynaecological (GYN) GEC ESTRO working group (II): concepts and terms in 3D image-based treatment planning in cervix cancer brachytherapy-3D dose volume parameters and aspects of 3D image-based anatomy, radiation physics, radiobiology. *Radiother Oncol* 2006; 78: 67-77.
31. Deufel CL, Tian S, Yan BB et al. Automated applicator digitization for high-dose-rate cervix brachytherapy using image thresholding and density-based clustering. *Brachytherapy* 2020; 19: 111-118.
32. Hu H, Yang Q, Li J et al. Deep learning applications in automatic segmentation and reconstruction in CT-based cervix brachytherapy. *J Contemp Brachytherapy* 2021; 13: 325-330.
33. Shaaer A, Paudel M, Smith M et al. Deep-learning-assisted algorithm for catheter reconstruction during MR-only gynecological interstitial brachytherapy. *J Appl Clin Med Phys* 2022; 23: e13494.
34. Moradi MM, Siavashpour Z, Takhtardeshir S et al. Fully automatic reconstruction of prostate high dose rate brachytherapy interstitial needles by using two phases deep learning based segmentation and object tracking algorithms, April 2022. https://doi.org/10.21203/rs.3.rs-1590410/v1.
35. Peroni M, Spadea MF, Riboldi M et al. Validation of automatic contour propagation for 4D treatment planning using multiple metrics. *Technol Cancer Res Treat* 2013; 12: 501-510.
36. Yoganathan SA, Paul SN, Paloor S et al. Automatic segmentation of magnetic resonance images for high-dose-rate cervical cancer brachytherapy using deep learning. *Med Phys* 2022; 49: 1571-1584.
37. Schindel J, Zhang W, Bhatia SK et al. Dosimetric impacts of applicator displacements and applicator reconstruction-uncertainties on 3D image-guided brachytherapy for cervical cancer. *J Contemp Brachytherapy* 2013; 5: 250-257.